

# DiMoSR: Feature Modulation via Multi-Branch Dilated Convolutions for Efficient Image Super-Resolution

M. Akın Yılmaz<sup>1</sup>  
mustafaakinyilmaz@ku.edu.tr

Ahmet Bilican<sup>1, 2</sup>  
abilican21@ku.edu.tr

A. Murat Tekalp<sup>3</sup>  
<https://mysite.ku.edu.tr/mtekalp/>

<sup>1</sup> Codeway AI Research  
Istanbul, TR

<sup>2</sup> Koç University  
Istanbul, TR

<sup>3</sup> KUIS AI Center, Koç University  
Istanbul, TR

## Abstract

Balancing reconstruction quality versus model efficiency remains a critical challenge in lightweight single image super-resolution (SISR). Despite the prevalence of attention mechanisms in recent state-of-the-art SISR approaches that primarily emphasize or suppress feature maps, alternative architectural paradigms warrant further exploration. This paper introduces DiMoSR (Dilated Modulation Super-Resolution), a novel architecture that enhances feature representation through modulation to complement attention in lightweight SISR networks. The proposed approach leverages multi-branch dilated convolutions to capture rich contextual information over a wider receptive field while maintaining computational efficiency. Experimental results demonstrate that DiMoSR outperforms state-of-the-art lightweight methods across diverse benchmark datasets, achieving superior PSNR and SSIM metrics with comparable or reduced computational complexity. Through comprehensive ablation studies, this work not only validates the effectiveness of DiMoSR but also provides critical insights into the interplay between attention mechanisms and feature modulation to guide future research in efficient network design. The code and model weights to reproduce our results are available at: <https://github.com/makinyilmaz/DiMoSR>.

## 1 Introduction

Single Image Super-Resolution (SISR) aims to reconstruct high-resolution (HR) images from low-resolution (LR) inputs by recovering lost details. It has gained increased attention due to advances in streaming media and high-definition devices, creating demand for efficient super-resolution methods across resource-constrained platforms. Deep learning has significantly advanced SISR [5, 19, 22, 28, 43, 44]. Leveraging the success of Transformer architectures in modeling long-range dependencies, Vision Transformer-based models have begun outperforming convolutional neural network (CNN)-based approaches [4, 6, 6, 13, 23, 40]. However, these sophisticated architectures often entail substantial computational

overhead, challenging their deployment in resource-limited environments. Numerous innovations have been proposed to reduce computational requirements [2, 3, 8, 9, 12, 15, 16, 18, 20, 21, 22, 27, 30, 31, 32, 33, 34, 35, 36, 38, 41, 42, 45], focusing on decreasing model parameters and floating-point operations. In lightweight models, spatial and channel attention have been effective mechanisms to enhance feature maps by emphasizing important parts while suppressing less significant ones. However, they typically operate within limited receptive fields, creating a trade-off between contextual awareness and efficiency. To address these limitations, we propose DiMoSR, which leverages multi-branch dilated convolutions for feature modulation that complements traditional spatial-channel attention. Using varying dilation rates, our approach captures broader contextual information while maintaining computational efficiency, combining the strengths of both approaches in lightweight scenarios.

Our contributions can be summarized as follows.

- 1) We introduce DiMoSR, a lightweight SISR architecture employing dilated convolutions for effective feature modulation across varying receptive fields.
- 2) We demonstrate through extensive experiments that DiMoSR outperforms state-of-the-art lightweight methods across multiple datasets while maintaining comparable or reduced computational complexity.
- 3) We present detailed ablation studies offering insights into the interplay between feature modulation and attention mechanisms, establishing design principles for future efficient super-resolution networks.

## 2 Related Work

### 2.1 Convolutional Neural Networks for SISR

Single Image Super-Resolution (SISR) has been revolutionized by deep learning approaches. The pioneering work SRCNN [2], demonstrated the potential of convolutional neural networks (CNN) for the super-resolution task. This was followed by FSRCNN [8], optimized for improved efficiency. VDSR [16] and EDSR [24] established the benefits of increased network depth, while ESPCN [30] introduced the efficient sub-pixel convolution operation for upsampling, now a standard component in modern SR methods. As the field progressed, architectures became more sophisticated, with networks such as RDN [44] leveraging dense connections, and RCAN [43] incorporating channel attention mechanisms. However, these improvements came at the cost of increased computational complexity, limiting deployment of these models in resource-constrained environments.

### 2.2 Lightweight Super-Resolution Networks

In response to the computational demands of deeper and heavier networks, research has focused on developing lightweight architectures that balance reconstruction quality with efficiency. CARN [2] proposed a cascading architecture with parameter sharing to reduce model size. IMDN [15] introduced an information multi-distillation mechanism that progressively extracts hierarchical features. PAN [45] presented a pixel attention network that applies attention at the pixel level, offering computational advantages. ECBSR [11] proposed edge-oriented convolution blocks designed for mobile devices. SMSR [65] explored sparsity by learning location-specific convolution kernels that adaptively focus on informative regions. Recent approaches include RLFN [18], which combined local feature extraction with residual

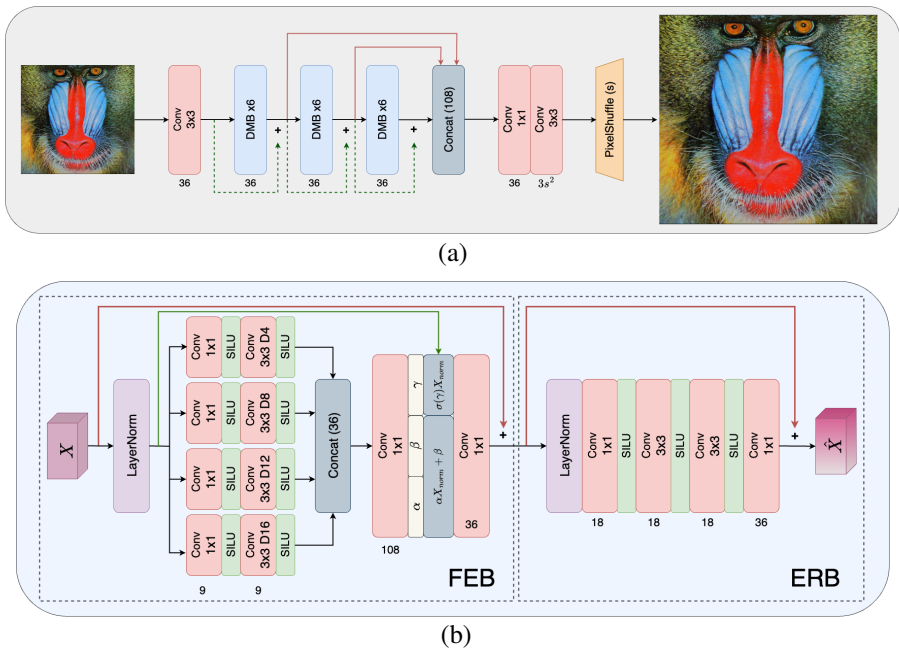


Figure 1: Our proposed DiMoSR framework: a) Architecture consisting of Dilated Modulation Blocks (DMBs), (b) Inside of a single DMB. It consists of a feature enhancement block (FEB) followed by an efficient residual block (ERB).

learning, LESRCNN[53], which enhanced basic CNN architectures, FDIW[42], which introduced feature distillation interaction weighting, and FMEN[9], which focused on memory efficiency alongside computational performance.

### 2.3 Attention Mechanisms in Super-Resolution

Attention mechanisms have significantly influenced super-resolution model design by enabling networks to focus on informative features. While initially focused on the channel dimension in works such as RCAN[43], attention has evolved to encompass both spatial and channel dimensions. HAN [28] introduced holistic attention that combines channel and spatial attention. For lightweight scenarios, attention has been adapted to minimize computational overhead. MAFFSRN[47] proposed multi-attention blocks with reduced complexity. SAFMN[62] introduced spatially-adaptive feature modulation with fewer parameters. SPAN[34] presented a parameter-free attention network that achieves efficiency through algorithmic innovations.

### 2.4 Feature Enhancement Strategies

Recent advances have explored alternative approaches to feature enhancement beyond conventional attention mechanisms. Blueprint[42] introduced a separable residual network architecture that reorganizes feature channels to improve information propagation while reducing redundancy. ShuffleMixer[61] proposed an innovative feature mixing strategy com-

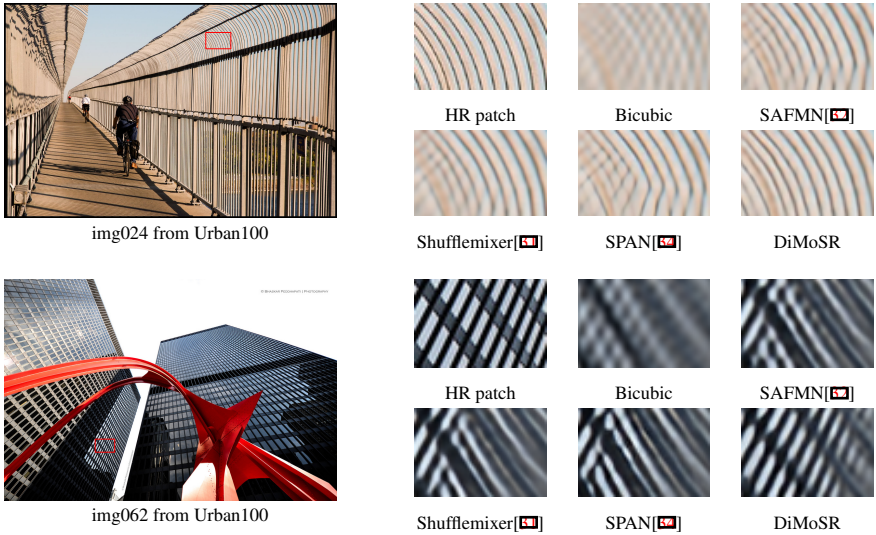


Figure 2: Visual comparison on two Urban100 images. Left: full-size images with marked zoom-in regions. Right: HR ground truth and SR results.

binning channel shuffling with targeted enhancement, creating diverse feature representations that capture complementary information. SAFMN[57] introduced spatially-adaptive feature manipulation techniques that dynamically adjust representations based on local content characteristics. While feature-wise linear modulation techniques[29] have shown effectiveness in other vision tasks, their adaptation to super-resolution has been limited. Our work addresses this gap by introducing a dilated modulation framework that leverages multi-scale contextual information without significant computational overhead, providing a complementary approach particularly well-suited for resource-constrained environments.

### 3 Method

We first provide an overview of the proposed Dilated Modulation Super-Resolution (DiMoSR) architecture for lightweight SISR, followed by detailed descriptions of its key components: the Dilated Modulation Block (DMB), the Feature Enhancement Block (FEB), and the Efficient Residual Block (ERB).

#### 3.1 Overview of Network Architecture

The overall architecture of our proposed DiMoSR network is depicted in Figure 1. Similar to most SISR networks, DiMoSR consists of three main components: (1) a shallow feature extraction module, (2) a deep feature extraction module with multiple DMBs, and (3) an image reconstruction module. Given a low-resolution (LR) input image  $I_{LR} \in \mathbb{R}^{H \times W \times 3}$ , we first apply a  $3 \times 3$  convolutional layer to extract shallow features  $\mathbb{R}^{H \times W \times C}$  where  $C = 36$  is the number of channels in feature maps. The extracted shallow features are then fed into a deep feature extraction module consisting of a sequence of DMBs with residual connections. We organize the DMBs in a specific structure where a group of DMBs is followed by a

residual connection. Specifically, after each sequence of 6 DMBs, we add the input features to the output features through a skip connection. This process is repeated 3 times, with each block’s output becoming the input to the next block. After processing through all the DMB groups, the features are concatenated and passed through a  $1 \times 1$  convolution for feature fusion. Finally, we reconstruct the super-resolved image  $I_{SR} \in \mathbb{R}^{sH \times sW \times 3}$  using a sequence of  $1 \times 1$  convolution,  $3 \times 3$  convolution, and a pixel shuffle operation[60] where  $s$  is the upscaling factor.

## 3.2 Dilated Modulation Block (DMB)

The core of our DiMoSR architecture is the DMB, which consists of two components: the Feature Enhancement Block (FEB) and the Efficient Residual Block (ERB). These components create a powerful mechanism for feature extraction, modulation, and attention that is both effective and computationally efficient.

### 3.2.1 Feature Enhancement Block (FEB)

The FEB, shown on the left side of Figure 1 (b), consists of multiple parallel branches with convolutional layers followed by SiLU activation functions. After a LayerNorm operation on the input features, the FEB processes them through four parallel branches, each containing a  $1 \times 1$  convolution followed by SiLU[14] activation and a  $3 \times 3$  dilated convolution with different dilation rates (D4, D8, D12, D16). This multi-branch structure allows the network to capture information at different receptive fields. The outputs from all branches are concatenated into  $F_{concat}$  and processed through  $1 \times 1$  convolutions to determine the modulation coefficients  $\alpha$  and  $\beta$ , and the attention weight  $\sigma(\gamma)$  where  $\sigma$  represents the sigmoid activation of  $\gamma$ . The process works as follows:

$$\alpha, \beta, \gamma = \text{Conv}1 \times 1(F_{concat}).\text{chunk}(3) \quad (1)$$

These parameters are then applied to the layer-normalized input  $X_{norm}$  to produce modulation and attention applied outputs:

$$\begin{aligned} \text{out1} &= \alpha X_{norm} + \beta \\ \text{out2} &= \sigma(\gamma) X_{norm} \end{aligned} \quad (2)$$

Finally, these two outputs are concatenated and fused through another  $1 \times 1$  convolution. A residual connection is added to complete the Feature Enhancement Block:

$$X_{FEB} = X + \text{Conv}_{1 \times 1}(\text{Concat}([\text{out1}, \text{out2}])) \quad (3)$$

This combined approach allows the network to both modulate feature strengths and focus attention on the most relevant features while preserving input information through the residual connection.

### 3.2.2 Efficient Residual Block (ERB)

The right side of Figure 1 (b) shows our Efficient Residual Block (ERB), which takes the output from the FEB as its input. The ERB follows a residual block structure for effective feature processing. After a LayerNorm operation on the input features, the ERB first maps them to

Table 1: **Benchmarking of Efficient Super-Resolution Networks** All PSNR and SSIM metrics are calculated using only the Y-channel. #FLOPs are measured for high-resolution output images of  $1280 \times 720$  pixels. **Red** and **Blue** colors indicate the best and second-best performances, respectively.

Methods	Scale	#Params [K]	#FLOPs [G]	Set5	Set14	B100	Urban100
Bicubic		-	-	33.66/0.9299	30.24/0.8688	29.56/0.8431	26.88/0.8403
SRCNN[ <b>Q</b> ]		57	53	36.66/0.9542	32.42/0.9063	31.36/0.8879	29.50/0.8946
FSRCNN[ <b>B</b> ]		12	6	37.00/0.9558	32.63/0.9088	31.53/0.8920	29.88/0.9020
ESPCN[ <b>Q</b> ]		21	5	36.83/0.9564	32.40/0.9096	31.29/0.8917	29.48/0.8975
VDSR[ <b>Q</b> ]		665	613	37.53/0.9587	33.03/0.9124	31.90/0.8960	30.76/0.9140
LapSRN[ <b>Q</b> ]		813	30	37.52/0.9590	33.08/0.9130	31.80/0.8950	30.41/0.9100
CARN[ <b>Q</b> ]		1592	223	37.76/0.9590	33.52/0.9166	32.09/0.8978	31.92/0.9256
EDSR-baseline[ <b>Q</b> ]		1370	316	37.99/0.9604	33.57/0.9175	32.16/0.8994	31.98/0.9272
IMDN[ <b>Q</b> ]		694	159	38.00/0.9605	33.63/0.9177	32.19/0.8996	32.17/0.9283
PAN[ <b>Q</b> ]	$\times 2$	261	71	38.00/0.9605	33.59/0.9181	32.18/0.8997	32.01/0.9273
LAPAR-A[ <b>Q</b> ]		548	171	38.01/0.9605	33.62/0.9183	32.19/0.8999	32.10/0.9283
MAFFSRN[ <b>Q</b> ]		402	86	37.97/0.9603	33.49/0.9170	32.14/0.8994	31.96/0.9268
SMSR[ <b>Q</b> ]		985	132	38.00/0.9601	33.64/0.9179	32.17/0.8990	32.19/0.9284
ECBSR[ <b>Q</b> ]		596	137	37.90/ <b>0.9615</b>	33.34/0.9178	32.10/ <b>0.9018</b>	31.71/0.9250
RLFN[ <b>Q</b> ]		527	116	<b>38.07/0.9607</b>	<b>33.72/0.9187</b>	<b>32.22/0.9000</b>	<b>32.33/0.9299</b>
ShuffleMixer[ <b>Q</b> ]		394	91	38.01/0.9606	33.63/0.9180	32.17/0.8995	31.89/0.9257
SAFMN[ <b>Q</b> ]		228	52	38.00/0.9605	33.54/0.9177	32.16/0.8995	31.84/0.9256
SPAN[ <b>Q</b> ]		481	94	<b>38.08/0.9608</b>	33.71/0.9183	<b>32.22/0.9002</b>	32.24/0.9294
DiMoSR-S		<b>239</b>	<b>54</b>	38.02/0.9606	33.67/0.9185	<b>32.22/0.9002</b>	32.16/0.9283
DiMoSR (Ours)		<b>338</b>	<b>76</b>	38.06/0.9607	<b>33.74/0.9194</b>	<b>32.24/0.9006</b>	<b>32.30/0.9295</b>
Bicubic		-	-	28.42/0.8104	26.00/0.7027	25.96/0.6675	23.14/0.6577
SRCNN[ <b>Q</b> ]		57	53	30.48/0.8628	27.49/0.7503	26.90/0.7101	24.52/0.7221
FSRCNN[ <b>B</b> ]		12	5	30.71/0.8657	27.59/0.7535	26.98/0.7150	24.62/0.7280
ESPCN[ <b>Q</b> ]		25	1	30.52/0.8697	27.42/0.7606	26.87/0.7216	24.39/0.7241
VDSR[ <b>Q</b> ]		665	613	31.35/0.8838	28.01/0.7674	27.29/0.7251	25.18/0.7524
LapSRN[ <b>Q</b> ]		813	149	31.54/0.8850	28.19/0.7720	27.32/0.7280	25.21/0.7560
CARN[ <b>Q</b> ]		1592	91	32.13/0.8937	28.60/0.7806	27.58/0.7349	26.07/0.7837
EDSR-baseline[ <b>Q</b> ]		1518	114	32.09/0.8938	28.58/0.7813	27.57/0.7357	26.04/0.7849
IMDN[ <b>Q</b> ]		715	41	32.21/0.8948	28.58/0.7811	27.56/0.7353	26.04/0.7838
PAN[ <b>Q</b> ]	$\times 4$	272	28	32.13/0.8948	28.61/0.7822	27.59/0.7363	26.11/0.7854
LAPAR-A[ <b>Q</b> ]		659	94	32.15/0.8944	28.61/0.7818	27.61/0.7366	26.14/0.7871
MAFFSRN[ <b>Q</b> ]		441	24	32.18/0.8948	28.58/0.7812	27.57/0.7361	26.04/0.7848
SMSR[ <b>Q</b> ]		1006	42	32.12/0.8932	28.55/0.7808	27.55/0.7351	26.11/0.7868
ECBSR[ <b>Q</b> ]		603	35	31.92/0.8946	28.34/0.7817	27.48/ <b>0.7393</b>	25.81/0.7773
RLFN[ <b>Q</b> ]		543	30	<b>32.24/0.8952</b>	28.62/0.7813	27.60/0.7364	26.17/0.7877
ShuffleMixer[ <b>Q</b> ]		411	28	32.21/ <b>0.8953</b>	<b>28.66/0.7827</b>	27.61/0.7366	26.08/0.7835
SAFMN[ <b>Q</b> ]		240	14	32.18/0.8948	28.60/0.7813	27.58/0.7359	25.97/0.7809
SPAN[ <b>Q</b> ]		498	24	32.20/ <b>0.8953</b>	<b>28.66/0.7834</b>	<b>27.62/0.7374</b>	<b>26.18/0.7879</b>
DiMoSR-S		<b>250</b>	<b>14</b>	32.24/0.8952	<b>28.66/0.7827</b>	<b>27.62/0.7374</b>	26.12/0.7847
DiMoSR		<b>349</b>	<b>20</b>	<b>32.31/0.8962</b>	<b>28.74/0.7844</b>	<b>27.65/0.7384</b>	<b>26.25/0.7889</b>

a lower channel dimension using a  $1 \times 1$  convolution for improved efficiency. These reduced features are then processed through  $3 \times 3$  convolution layers, and finally, another  $1 \times 1$  convolution is applied to increase the channel count back to match the input feature dimensions. Similar to the FEB, SiLU activation functions are applied between each convolution layer.

The ERB process can be formulated as:

$$\hat{X} = X_{FEB} + \text{ERB}(\text{LayerNorm}(X_{FEB})), \quad (4)$$

where  $X_{FEB}$  represents the features from the Feature Enhancement Block and  $\text{ERB}(\cdot)$  represents the operations performed by the Efficient Residual Block. The final residual connection helps preserve information flow and stabilize training.

The complementary ERB pathway provides a computationally efficient feature processing stream that works alongside the more complex attention and modulation mechanisms of the FEB. While the FEB focuses on applying attention and modulation operations to enhance features, the ERB handles the direct feature processing through its efficient design.

Table 2: Effect of attention mechanism and feature modulation components on  $\times 4$  upscaling. Results are presented as PSNR/SSIM across four benchmark datasets.

Attention	Feature Modulation	Set5	Set14	B100	Urban100
$\times$	$\times$	31.94/0.8920	28.50/0.7795	27.51/0.7336	25.80/0.7743
$\checkmark$	$\times$	32.28/0.8958	28.69/0.7834	27.63/0.7376	26.18/0.7867
$\times$	$\checkmark$	32.26/0.8959	28.69/0.7836	27.63/0.7376	26.14/0.7858
$\checkmark$	$\checkmark$	<b>32.31/0.8962</b>	<b>28.74/0.7844</b>	<b>27.65/0.7384</b>	<b>26.25/0.7889</b>

## 4 Experiments

In this section, we evaluate our proposed DiMoSR method through comprehensive experiments. We first outline the experimental setup, followed by comparisons with state-of-the-art methods and ablation studies where we analyze individual components of our approach.

### 4.1 Experimental Setup

**Datasets.** For training, we use DF2K dataset which is a combination of DIV2K[10] and Flickr2K[24] datasets, comprising a total of 3450 high-quality images with diverse content. Low-resolution (LR) inputs are generated by applying bicubic downscaling to the high-resolution (HR) reference images. We evaluate our model on four benchmark datasets: Set5[9], Set14[39], B100[26], and Urban100[14], representing a range of image types from natural scenes to urban environments.

**Evaluation Metrics.** Following standard practice, we measure reconstruction quality using Peak Signal-to-Noise Ratio (PSNR) and Structural Similarity Index (SSIM)[37]. All metrics are calculated on the Y channel in YCbCr color space.

**Training Details.** For training both our DiMoSR (36 channels and 18 DMBs) and its smaller sibling DiMoSR-S (32 channels and 16 DMBs), we applied data augmentation including random horizontal flips and  $90^\circ$ ,  $180^\circ$ , and  $270^\circ$  rotations. We randomly cropped patches of size  $128 \times 128$  pixels from LR images, corresponding to  $512 \times 512$  patches in HR images for  $\times 4$  upscaling. We optimized our models using Adam[17] optimizer with  $\beta_1 = 0.9$  and  $\beta_2 = 0.99$  for 500,000 iterations with a batch size of 24 pairs. The learning rate starts at  $1 \times 10^{-3}$  and decreases to  $1 \times 10^{-5}$  using Cosine Annealing[25]. Following[11, 31, 32], our loss function combines mean absolute error (MAE) and FFT-based frequency loss:

$$\mathcal{L}_{total} = \mathcal{L}_{MAE} + \lambda \mathcal{L}_{freq} \quad (5)$$

where  $\mathcal{L}_{MAE} = |I_{SR} - I_{HR}|$  is the pixel-wise MAE,  $\mathcal{L}_{freq} = |\mathcal{F}(I_{SR}) - \mathcal{F}(I_{HR})|$  is the frequency domain loss computed using Fast Fourier Transform (FFT), and  $\lambda = 0.05$  balances the two terms.

### 4.2 Comparison with State-of-the-Art Methods

We compare our DiMoSR method with various efficient super-resolution approaches across standard benchmark datasets for scale factors  $\times 2$ ,  $\times 4$  and present quantitative results in Table 1. For  $\times 2$  upscaling, DiMoSR outperforms many models with significantly higher

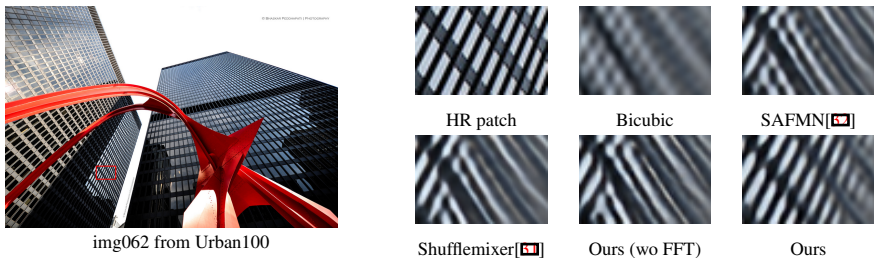


Figure 3: Visual comparison on img062 from Urban100 ( $\times 4$  upscaling). Note that SAFMN[52] and ShuffleMixer[51] were trained with FFT loss, yet our model without FFT loss achieves comparable results. Our complete model with FFT Loss demonstrates superior edge preservation and detail reconstruction, particularly in structural patterns.

parameter counts and computational costs, providing better PSNR values than RLFN, ShuffleMixer, and SPAN on several benchmarks.

Our performance is particularly notable for  $\times 4$  upscaling, where DiMoSR achieves state-of-the-art performance on all four benchmark datasets in terms of PSNR and on three of the four benchmark datasets in terms of SSIM. These results are achieved with significant efficiency gains compared to recent efficient SR methods that have more parameter count and FLOPs.

In particular, our lightweight variant DiMoSR-S for  $\times 2$  upscaling substantially outperforms SAFMN across all benchmark datasets despite having nearly identical computational requirements. For  $\times 4$  upscaling, DiMoSR-S achieves remarkable results on Set5 (32.24 dB), matching RLFN for the second-best performance while utilizing 54% fewer parameters and 53% fewer FLOPs. On Set14, DiMoSR-S (28.66 dB) achieves equivalent performance to ShuffleMixer and SPAN, securing joint second place despite requiring significantly reduced computational complexity. Compared to these competing architectures, DiMoSR-S demonstrates substantial efficiency gains of 39-50% in parameter count and 41.7-50% in floating-point operations while maintaining comparable or superior quantitative results across multiple benchmark datasets, including B100 (27.62 dB). These empirical findings conclusively demonstrate that our approach successfully addresses the fundamental challenge of achieving superior reconstruction quality while simultaneously reducing computational requirements.

## 4.3 Ablation Study

### 4.3.1 Feature Modulation and Attention

To validate both the attention mechanism and feature modulation components of our DiMoSR model we conduct comprehensive ablation studies analyzing the individual and combined contributions of the attention mechanism and feature modulation components in Table 2. When either component is disabled independently, we observe performance decreases across all benchmark datasets for  $\times 4$  upscaling. The most significant impact appears on the Urban100 dataset, where disabling attention causes a 0.10dB decrease compared to our full model. Disabling feature modulation similarly reduces performance across all datasets. When both components are enabled, we achieve the best performance across all datasets, demonstrating that attention and feature modulation mechanisms contribute significantly to

Table 3: Effect of FFT loss on  $\times 4$  upscaling. Results are presented as PSNR/SSIM across four benchmark datasets.

MAE	FFT Loss	Set5	Set14	B100	Urban100
✓	✗	32.26/0.8957	28.65/0.7829	27.62/0.7375	26.15/0.7884
✓	✓	<b>32.31/0.8962</b>	<b>28.74/0.7844</b>	<b>27.65/0.7384</b>	<b>26.25/0.7889</b>

DiMoSR’s overall performance. Their combined effect is particularly beneficial for images with complex structures, as evidenced on the Urban100 dataset.

### 4.3.2 FFT Loss

To evaluate the effectiveness of the frequency domain loss function, we conduct an ablation study on the impact of FFT loss in our DiMoSR model. Table 3 presents a comparison between training with standard MAE only versus combining MAE with FFT loss using a weighting factor of 0.05. We observe notable performance improvements for  $\times 4$  upscaling across all benchmark datasets when introducing the FFT loss component along with the standard MAE.

Figure 3 provides visual evidence of the FFT loss impact on reconstruction quality. While our base model without FFT loss already performs comparably to other state-of-the-art models that utilize FFT loss (SAFMN and ShuffleMixer), integrating FFT loss into our DiMoSR model produces substantially improved visual results. The zoomed-in regions clearly demonstrate that adding FFT loss helps recover more accurate high-frequency details and sharper edges, particularly in structures with complex patterns, as found in urban scenes. These results demonstrate that the frequency domain loss complements the spatial domain supervision provided by the MAE, resulting in better visual quality and quantitative metrics across diverse image content.

## 5 Conclusion

This paper introduces DiMoSR, a novel lightweight super-resolution network that leverages multi-branch dilated convolutions and feature modulation to achieve efficient and high-quality image super-resolution. Extensive experiments on benchmark datasets demonstrate that DiMoSR consistently outperforms state-of-the-art lightweight SR methods, particularly for the challenging  $\times 4$  upscaling task. Even our smaller variant, DiMoSR-S, delivers competitive performance while requiring significantly fewer computational resources than comparable methods. Both models achieve superior PSNR and SSIM metrics across multiple datasets compared to alternatives with higher computational demands. Our ablation studies confirm that both attention and feature modulation components contribute significantly to the overall performance, with their combined effect showing particular benefits for complex image structures. The success of DiMoSR highlights the potential of alternative feature enhancement approaches beyond traditional attention mechanisms for lightweight super-resolution networks.

## References

- [1] Eirikur Agustsson and Radu Timofte. Ntire 2017 challenge on single image super-resolution: Dataset and study. In *IEEE/CVF Conf. on Computer Vision and Patt. Recog. Workshops (CVPRW)*, pages 1122–1131, 2017. doi: 10.1109/CVPRW.2017.150.
- [2] Namhyuk Ahn, Byungkon Kang, and Kyung-Ah Sohn. Fast, accurate, and lightweight super-resolution with cascading residual network. In *Euro. Conf. Computer Vision (ECCV)*, pages 256–272, 2018.
- [3] Marco Bevilacqua, Aline Roumy, Christine Guillemot, and Marie-Line Alberi Morel. Low-Complexity Single-Image Super-Resolution based on Nonnegative Neighbor Embedding. In *British Machine Vision Conference (BMVC)*, Guildford, Surrey, UK, September 2012. URL <https://inria.hal.science/hal-00747054>.
- [4] Xiangyu Chen, Xintao Wang, Jiantao Zhou, Yu Qiao, and Chao Dong. Activating more pixels in image super-resolution transformer. In *IEEE/CVF Conf. on Comp. Vis. Patt. Recog. (CVPR)*, pages 22367–22377, 2023. doi: 10.1109/CVPR52729.2023.02142.
- [5] Zheng Chen, Yulun Zhang, Jinjin Gu, Linghe Kong, Xiaokang Yang, and Fisher Yu. Dual aggregation transformer for image super-resolution. In *ICCV*, 2023.
- [6] Zheng Chen, Yulun Zhang, Jinjin Gu, Linghe Kong, and Xiaokang Yang. Recursive generalization transformer for image super-resolution. In *ICLR*, 2024.
- [7] Chao Dong, Chen Change Loy, Kaiming He, and Xiaoou Tang. Image super-resolution using deep convolutional networks. *IEEE Transactions on Pattern Analysis and Machine Intelligence*, 38(2):295–307, 2016. doi: 10.1109/TPAMI.2015.2439281.
- [8] Chao Dong, Chen Change Loy, and Xiaoou Tang. Accelerating the super-resolution convolutional neural network. In *European Conference Computer Vision (ECCV)*, pages 391–407. Springer International Publishing, 2016. ISBN 978-3-319-46475-6.
- [9] Zongcai Du, Ding Liu, Jie Liu, Jie Tang, Gangshan Wu, and Lean Fu. Fast and memory-efficient network towards efficient image super-resolution. In *IEEE/CVF Conf. on Computer Vision and Patt. Recog. Workshops (CVPRW)*, pages 852–861, 2022. doi: 10.1109/CVPRW56347.2022.00101.
- [10] Stefan Elfving, Eiji Uchibe, and Kenji Doya. Sigmoid-weighted linear units for neural network function approximation in reinforcement learning. *Neural Networks*, 107:3–11, 2018. ISSN 0893-6080. doi: <https://doi.org/10.1016/j.neunet.2017.12.012>. URL <https://www.sciencedirect.com/science/article/pii/S0893608017302976>. Special issue on deep reinforcement learning.
- [11] Dario Fuoli, Luc Van Gool, and Radu Timofte. Fourier space losses for efficient perceptual image super-resolution. In *IEEE/CVF Int. Conf. on Computer Vision (ICCV)*, pages 2340–2349, 2021. doi: 10.1109/ICCV48922.2021.00236.
- [12] Guangwei Gao, Wenjie Li, Juncheng Li, Fei Wu, Huimin Lu, and Yi Yu. Feature distillation interaction weighting network for lightweight image super-resolution. In *AAAI Conf. on Artificial Intelligence*, volume 36, pages 661–669, 2022.

- [13] Chih-Chung Hsu, Chia-Ming Lee, and Yi-Shiuan Chou. Drct: Saving image super-resolution away from information bottleneck. In *IEEE/CVF Conf. on Computer Vision and Pattern Recognition (CVPR) Workshops*, pages 6133–6142, June 2024.
- [14] Jia-Bin Huang, Abhishek Singh, and Narendra Ahuja. Single image super-resolution from transformed self-exemplars. In *IEEE/CVF Conf. on Computer Vision and Pattern Recognition (CVPR)*, pages 5197–5206, 2015. doi: 10.1109/CVPR.2015.7299156.
- [15] Zheng Hui, Xinbo Gao, Yunchu Yang, and Xiumei Wang. Lightweight image super-resolution with information multi-distillation network. In *ACM Int. Conf. on Multimedia (ACM MM)*, pages 2024–2032, 2019.
- [16] Jiwon Kim, Jung Kwon Lee, and Kyoung Mu Lee. Accurate image super-resolution using very deep convolutional networks. In *IEEE/CVF Conf. on Computer Vision and Pattern Recognition (CVPR)*, pages 1646–1654, 2016. doi: 10.1109/CVPR.2016.182.
- [17] Diederik P. Kingma and Jimmy Ba. Adam: A method for stochastic optimization. In *Int. Conf. Learning Representation (ICLR)*, 2015.
- [18] Fangyuan Kong, Mingxi Li, Songwei Liu, Ding Liu, Jingwen He, Yang Bai, Fangmin Chen, and Lean Fu. Residual local feature network for efficient super-resolution. In *IEEE/CVF Conf. on Computer Vision and Patt. Recog. Workshops (CVPRW)*, pages 765–775, 2022. doi: 10.1109/CVPRW56347.2022.00092.
- [19] Cansu Korkmaz, A. Murat Tekalp, and Zafer Dogan. Training transformer models by wavelet losses improves quantitative and visual performance in single image super-resolution. In *IEEE/CVF Conf. on Comp. Vision and Patt. Recog. (CVPR)*, June 2024.
- [20] Wei-Sheng Lai, Jia-Bin Huang, Narendra Ahuja, and Ming-Hsuan Yang. Deep laplacian pyramid networks for fast and accurate super-resolution. In *IEEE Conf. on Computer Vision and Patt. Recog. (CVPR)*, pages 5835–5843, 2017. doi: 10.1109/CVPR.2017.618.
- [21] Wenbo Li, Kun Zhou, Lu Qi, Nianjuan Jiang, Jiangbo Lu, and Jiaya Jia. Lappar: Linearly-assembled pixel-adaptive regression network for single image super-resolution and beyond. *Advances in Neural Information Processing Systems*, 33, 2020.
- [22] Zheyuan Li, Yingqi Liu, Xiangyu Chen, Haoming Cai, Jinjin Gu, Yu Qiao, and Chao Dong. Blueprint separable residual network for efficient image super-resolution. In *IEEE/CVF Conf. on Computer Vision and Pattern Recognition Workshops (CVPRW)*, pages 832–842, 2022. doi: 10.1109/CVPRW56347.2022.00099.
- [23] Jingyun Liang, Jiezhong Cao, Guolei Sun, Kai Zhang, Luc Van Gool, and Radu Timofte. Swinir: Image restoration using swin transformer. In *IEEE/CVF Int. Conf. on Computer Vision Workshops (ICCVW)*, pages 1833–1844, 2021. doi: 10.1109/ICCVW54120.2021.00210.
- [24] Bee Lim, Sanghyun Son, Heewon Kim, Seungjun Nah, and Kyoung Mu Lee. Enhanced deep residual networks for single image super-resolution. In *IEEE Conf. on Computer Vision and Patt. Recog. Workshops (CVPRW)*, pages 1132–1140, 2017. doi: 10.1109/CVPRW.2017.151.

- [25] Ilya Loshchilov and Frank Hutter. SGDR: Stochastic gradient descent with warm restarts. In *Int. Conf. on Learning Representations (ICLR)*, 2017.
- [26] D. Martin, C. Fowlkes, D. Tal, and J. Malik. A database of human segmented natural images and its application to evaluating segmentation algorithms and measuring ecological statistics. In *IEEE Int. Conf. on Computer Vision (ICCV)*, volume 2, pages 416–423, 2001. doi: 10.1109/ICCV.2001.937655.
- [27] Abdul Muqeet, Jiwon Hwang, Subin Yang, JungHeum Kang, Yongwoo Kim, and Sung-Ho Bae. Multi-attention based ultra lightweight image super-resolution. In *Euro. Conf. Computer Vision (ECCV) Workshops*, pages 103–118, 2020.
- [28] Ben Niu, Weilei Wen, Wenqi Ren, Xiangde Zhang, Lianping Yang, Shuzhen Wang, Kaihao Zhang, Xiaochun Cao, and Haifeng Shen. Single image super-resolution via a holistic attention network. In *Euro. Conf. Comp. Vision (ECCV)*, pages 191–207, 2020.
- [29] Ethan Perez, Florian Strub, Harm de Vries, Vincent Dumoulin, and Aaron C. Courville. Film: Visual reasoning with a general conditioning layer. In *AAAI*, 2018.
- [30] Wenzhe Shi, Jose Caballero, Ferenc Huszár, Johannes Totz, Andrew P. Aitken, Rob Bishop, Daniel Rueckert, and Zehan Wang. Real-time single image and video super-resolution using an efficient sub-pixel convolutional neural network. In *IEEE/CVF Conf. on Computer Vision and Pattern Recognition (CVPR)*, pages 1874–1883, 2016.
- [31] Long Sun, Jinshan Pan, and Jinhui Tang. ShuffleMixer: An efficient convnet for image super-resolution. In *Advances in Neural Information Processing Systems*, 2022.
- [32] Long Sun, Jiangxin Dong, Jinhui Tang, and Jinshan Pan. Spatially-adaptive feature modulation for efficient image super-resolution. In *ICCV*, 2023.
- [33] Chunwei Tian, Ruibin Zhuge, Zhihao Wu, Yong Xu, Wangmeng Zuo, Chen Chen, and Chia-Wen Lin. Lightweight image super-resolution with enhanced cnn. *Knowledge-Based Systems*, page 106235, 2020.
- [34] Cheng Wan, Hongyuan Yu, Zhiqi Li, Yihang Chen, Yajun Zou, Yuqing Liu, Xuanwu Yin, and Kunlong Zuo. Swift parameter-free attention network for efficient super-resolution. In *IEEE/CVF Conf. on Computer Vision and Pattern Recognition (CVPR)*, pages 6246–6256, 2024.
- [35] Longguang Wang, Xiaoyu Dong, Yingqian Wang, Xinyi Ying, Zaiping Lin, Wei An, and Yulan Guo. Exploring sparsity in image super-resolution for efficient inference. In *IEEE/CVF Conf. on Comp. Vision and Patt. Recog. (CVPR)*, pages 4915–4924, 2021.
- [36] Shanqin Wang, Miao Zhang, and Mengjun Miao. The super-resolution reconstruction algorithm of multi-scale dilated convolution residual network. *Frontiers in Neurorobotics*, Volume 18, 2024. doi: 10.3389/fnbot.2024.1436052. URL <https://www.frontiersin.org/journals/neurorobotics/articles/10.3389/fnbot.2024.1436052>.
- [37] Zhou Wang, A.C. Bovik, H.R. Sheikh, and E.P. Simoncelli. Image quality assessment: from error visibility to structural similarity. *IEEE Transactions on Image Processing*, 13(4):600–612, 2004. doi: 10.1109/TIP.2003.819861.

- [38] Eduard Zamfir, Zongwei Wu, Nancy Mehta, Yulun Zhang, and Radu Timofte. See more details: Efficient image super-resolution by experts mining. In *Int. Conf. on Machine Learning (ICML)*. PMLR, 2024.
- [39] Roman Zeyde, Michael Elad, and Matan Protter. On single image scale-up using sparse-representations. In *Curves and Surfaces*, pages 711–730, Berlin, Heidelberg, 2012. Springer Berlin Heidelberg. ISBN 978-3-642-27413-8.
- [40] Dafeng Zhang, Feiyu Huang, Shizhuo Liu, Xiaobing Wang, and Zhezhu Jin. Swinfir: Revisiting the swinir with fast fourier convolution and improved training for image super-resolution. *arXiv preprint arXiv:2208.11247*, 2022.
- [41] Xindong Zhang, Hui Zeng, and Lei Zhang. Edge-oriented convolution block for real-time super resolution on mobile devices. In *ACM Int. Conf. on Multimedia*, pages 4034–4043, 2021.
- [42] Xindong Zhang, Hui Zeng, Shi Guo, and Lei Zhang. Efficient long-range attention network for image super-resolution. In *European Conf. on Computer Vision*, 2022.
- [43] Yulun Zhang, Kunpeng Li, Kai Li, Lichen Wang, Bineng Zhong, and Yun Fu. Image super-resolution using very deep residual channel attention networks. In *ECCV*, 2018.
- [44] Yulun Zhang, Yapeng Tian, Yu Kong, Bineng Zhong, and Yun Fu. Residual dense network for image super-resolution. In *CVPR*, 2018.
- [45] Hengyuan Zhao, Xiangtao Kong, Jingwen He, Yu Qiao, and Chao Dong. Efficient image super-resolution using pixel attention. In *European Conf. on Computer Vision*, pages 56–72. Springer, 2020.